



**HAL**  
open science

# Novel RANK Antagonists for the Treatment of Bone-Resorptive Disease: Theoretical Predictions and Experimental Validation

Stéphane Téletchéa, Verena Stresing, Soizic Hervouet, Marc Baud'Huin, Marie-Françoise Heymann, Gildas Bertho, Céline Charrier, Kosei Ando, Dominique Heymann

## ► To cite this version:

Stéphane Téletchéa, Verena Stresing, Soizic Hervouet, Marc Baud'Huin, Marie-Françoise Heymann, et al.. Novel RANK Antagonists for the Treatment of Bone-Resorptive Disease: Theoretical Predictions and Experimental Validation. *Journal of Bone and Mineral Research*, 2014, 29 (6), pp.1466 - 1477. 10.1002/jbmr.2170 . inserm-01644748

**HAL Id: inserm-01644748**

**<https://inserm.hal.science/inserm-01644748>**

Submitted on 22 Nov 2017

**HAL** is a multi-disciplinary open access archive for the deposit and dissemination of scientific research documents, whether they are published or not. The documents may come from teaching and research institutions in France or abroad, or from public or private research centers.

L'archive ouverte pluridisciplinaire **HAL**, est destinée au dépôt et à la diffusion de documents scientifiques de niveau recherche, publiés ou non, émanant des établissements d'enseignement et de recherche français ou étrangers, des laboratoires publics ou privés.

**Novel RANK antagonists for the treatment of bone resorptive disease:  
Theoretical predictions and experimental validation**

**Stéphane Téletchéa<sup>1\*</sup>, Verena Stresing<sup>1\*</sup>, Soizic Hervouet<sup>1</sup>, Marc Baud'huin<sup>1,2</sup>, Marie-Françoise Heymann<sup>1,2</sup>, Gildas Bertho<sup>3</sup>, Céline Charrier<sup>1</sup>, Kosei Ando<sup>1</sup>, Dominique Heymann<sup>1,2</sup>**

<sup>1</sup>INSERM, UMR 957, Equipe labellisée LIGUE 2012, Université de Nantes, LPRO (Laboratory of the Physiopathology of Bone Resorption and Therapy of Primary Bone Tumors), Nantes, France, <sup>2</sup>Nantes Hospital, France, <sup>3</sup>CNRS UMR8601, Université Paris Descartes, Paris, France.

\*S.T. and V.S. contributed equally to this work.

**Authors major degree:** Stéphane Téletchéa, Ph.D.; Verena Stresing, Ph.D.; Soizic Hervouet, B.Sc.; Marc Baud'huin, Pharm. D., Ph.D.; Marie-Françoise Heymann, M.D., Ph.D.; Gildas Bertho, Ph.D.; Céline Charrier, B.Sc.; Kosei Ando, M.D., Ph.D.; Dominique Heymann, Ph.D.

**Grant support:** This study was supported by the Fond Unique Interministeriel n°08 90 6214 (GELTOP project) and the Ligue Nationale Contre le Cancer (Equipe LIGUE 2012). K. Ando received a postdoctoral fellowship from the Region des Pays de La Loire (France).

**Correspondance:** Dominique Heymann, INSERM UMR 957, Faculté de Médecine, Université de Nantes, 1 rue Gaston Veil, 44035 Nantes, France. Phone: +33240412845; Fax: +33240412860; Email: dominique.heyman@univ-nantes.fr

**Disclosure:** All authors state that they have no conflicts of interest. Pep8 and Pep8 derivatives have been filed under patent number EP11306766.4 – 210.

Additional Supporting Information may be found in the online version of this article.

## **Abstract**

Receptor activator of nuclear factor- $\kappa$ B (RANK) and RANK ligand play a pivotal role in bone metabolism, and selective targeting of RANK signaling has become a promising therapeutic strategy in the management of resorptive bone diseases. Existing antibody-based therapies and novel inhibitors currently in development were designed to target the ligand, rather than the membrane receptor expressed on osteoclast precursors. We describe here an alternative approach to designing small peptides able to specifically bind to the hinge region of membrane RANK responsible for the conformational change upon RANKL association. A nonapeptide generated by this method was validated for its biological activity *in vitro* and *in vivo* and served as a lead compound for the generation of a series of peptide RANK antagonists derived from the original sequence. Our study presents a structure- and knowledge based strategy for the design of novel effective and affordable small peptide inhibitors specifically targeting the receptor RANK and opens a new therapeutic opportunity for the treatment of resorptive bone-disease.

**Key words:** bone resorption, drug design, RANK, RANKL, peptide inhibitors

## INTRODUCTION

Bone tissue undergoes constant remodeling to fulfill its principal functions of mechanical support, maintenance of calcium homeostasis, and as a stem cell supplier<sup>(1)</sup>. Receptor activator of nuclear factor- $\kappa$ B (RANK) and its ligand RANKL are two key proteins of bone remodeling that coordinate the interaction between bone resorbing osteoclasts and bone forming osteoblasts.<sup>(2-4)</sup> Osteoprotegerin (OPG), primarily secreted by bone stromal cells, acts as a decoy receptor to prevent RANKL from binding RANK,<sup>(5)</sup> and the dysregulation of the RANKL/RANK/OPG system causes an imbalance in bone homeostasis and results in various bone disorders.<sup>(6;7)</sup>

Because of the crucial role of this molecular triad, selective targeting of RANK signaling has become a promising strategy for the management of bone resorptive diseases.<sup>(8)</sup> For example, the chimeric protein RANK-Fc,<sup>(9;10)</sup> the RANKL inhibitor OPG<sup>(11;12)</sup> or formulated siRNAs targeting Rankl<sup>(13)</sup> showed promising results in the treatment of tumor-associated osteolysis. Denosumab, a fully human monoclonal antibody against RANKL, is the first RANKL inhibitor approved for the treatment of osteoporosis and the prevention of skeleton-related events in patients with bone metastases.<sup>(14;15)</sup> However, the high cost of these antibody-driven therapies and side effects may limit their widespread use.<sup>(16;17)</sup>

An alternative approach is the use of biocompatible inhibitory peptides targeting specific receptor-ligand interactions. The classical structure-based method to designing therapeutic peptides is based on the amino acid (AA) sequences found at protein-protein interaction sites. When no structural information is available, a comparative model can be built using another member of the protein family as a template to derive inhibitory peptides based on the predicted interaction zone. This approach was successfully applied to various members of the TNF family,<sup>(18-20)</sup> such as the peptide WP9QY, initially designed to target the TNF $\alpha$ /TNFR interaction, and the OPG mimetic OP3-4. The crystal structure determinations of RANKL,

RANK and RANK complexed with RANKL<sup>(21;22)</sup> provided detailed insights into the key structural features that govern the specific ligand-receptor recognition, and led to the development of novel inhibitory peptidomimetics containing key residues of the receptor-ligand interface with a mild to strong selectivity for their target.<sup>(22;23)</sup> However, most active inhibitors targeted the ligand, not the receptor. Since regulation of RANK, unlike RANKL expression, is controlled by only a few modulators<sup>(24)</sup> targeting the receptor seemed a logical approach for the design of new inhibitors.

Here, we present an alternative, structure-based approach for the design of small peptide inhibitors<sup>(25)</sup> able to specifically bind to the hinge region of membrane RANK, thereby blocking the RANK/RANKL interaction. A nonapeptide inhibitor generated by our method was further evaluated for its effect on osteoclast function in vitro and on ovariectomy-induced bone loss in vivo and served as a lead compound for the generation of a series of RANK antagonists, opening a new opportunity for the treatment of resorptive bone-disease.

## **MATERIALS AND METHODS**

***Generation of a peptide library***—A wide database of peptides of random amino acid sequences was generated in silico on a dual quad-core 2.66 Ghz Xeon 5630 workstation and filtered for aqueous solubility using a combination of biochemical and sequence-related filters (for details, see Supplemental Methods and **Fig. S1**). The resulting collection of  $22.5 \times 10^6$  peptides was processed to provide three-dimensional peptide coordinates. Each peptide was typed with the CHARMM<sup>(26)</sup> force-field for further analysis within Discovery Studio 2.5.5 (Accelrys Software).

**Docking experiments and refinement of docking poses**—The Human RANK-RANKL crystal structure<sup>(21)</sup> (PDB id: 3ME2) was used as a reference to define putative binding sites at the RANK-RANKL interaction site. Docking experiments were performed with peptides in the putative binding region on RANK using the CDOCKER<sup>(27)</sup> module of Discovery Studio 2.5.5 (**Fig. S1**). Principal poses were visually inspected and the most promising poses were refined manually for a better characterization of the most favorable RANK-peptide interactions.

**Surface plasmon resonance binding assay**—Biosensor experiments were carried out on a Biacore 3000 as published previously.<sup>(28)</sup> Recombinant RANKL or RANK-Fc (R&D Systems) was covalently immobilized to the dextran matrix of a Biacore CM5 sensor chip (flow rate: 5  $\mu$ L/min). Immobilization levels ranged from 400 to 3,000 response units (RU) for RANKL or 5,000 RU for RANK. Binding assays were performed at 25°C in 10 mM HEPES buffer, pH 7.4. Peptide binding to RANK or RANKL was determined using single cycle kinetics. The sensorgrams were fitted to calculate the equilibrium-dissociation constants using the Langmuir 1:1 model with BiaEval 4.1 software (Biacore).

**NMR Spectroscopy**—NMR experiments were run at 500.13 MHz for <sup>1</sup>H on a Bruker AVANCE 500 spectrometer with a Linux PC workstation, using 5-mm standard or 3-mm Shigemi tubes with magnetic susceptibilities matched to the solvent H<sub>2</sub>O/<sup>2</sup>H<sub>2</sub>O. Spectra of Pep8 (0.1-1 mM) were recorded in 200 mM sodium phosphate buffer (H<sub>2</sub>O/<sup>2</sup>H<sub>2</sub>O, 95:5), pH 7.4. 2D NMR spectra were recorded in the phase-sensitive mode using the States-TPPI method.<sup>(29)</sup> All experiments were carried out using the WATERGATE pulse sequence for water suppression or the excitation sculpting water suppression to eliminate the solvent signal.<sup>(30;31)</sup> 2D COSY, TOCSY and NOESY spectra were recorded at 280 K. TOCSY spectra were recorded using a MLEV-17 spin-

lock sequence (mixing time: 35 and 70 ms).<sup>(32)</sup> 2D NOESY experiments were recorded at 100 to 500 ms mixing times. Heteronuclear  $^1\text{H}^{13}\text{C}$  HSQC spectra were recorded at 280 K in the same conditions. For experiments with soluble RANK-Fc, ligand-to-protein ratios ranged from 100:1 to 1,000:1 (0.1-1 mM Pep8). Chemical shift assignments refer to internal 3-(trimethylsilyl) propionic-2,2,3,3-d<sub>4</sub> acid sodium salt (TSP-d<sub>4</sub>). TRNOESY spectra of Pep8 with RANK-Fc were recorded using a mixing time of 100 to 500 ms.

1D  $^1\text{H}$  STD NMR spectra of the peptide-protein mixtures were recorded at 500 MHz with 4K scans and selective saturation of protein resonances as described previously.<sup>(33)</sup> To enhance the saturation transfer efficiency, clean STD-NMR experiments<sup>(34)</sup> were combined with an optimized excitation  $90^\circ$  E-Burp-1 selective or  $90^\circ$  E-Burp-1 cosine modulated selective pulse.<sup>(35)</sup> The irradiation frequencies were set to -0.4/10.1/60 ppm ( $f_{\text{on1}}/f_{\text{on2}}/f_{\text{off}}$ ), the height of Gaussian-shaped pulses was set to 200 Hz and the near ligand resonances were >500 Hz. Subtraction of FID values with on- and off-resonance protein saturation was achieved by phase cycling. Relative STD values were calculated by dividing STD signal intensities by the intensities of the corresponding signals in a 1D  $^1\text{H}$  NMR reference spectrum of the same sample recorded with similar parameter conditions.

**Peptides and cell lines**—Peptides were purchased from GeneCust EUROPE and stored at  $-20^\circ\text{C}$  until use. 1 mM stock solutions were stored at  $-20^\circ\text{C}$  for up to two weeks, diluted solutions were freshly prepared and sterile filtered before use. Murine RAW264.7 cells (ATCC) were cultured in  $\alpha$ MEM/FBS-10%. Human embryonic kidney 293 cells stably expressing RANK (HEK-RANK cells, see Supplemental Methods) were maintained in DMEM/FBS-10% with 1  $\mu\text{g}/\text{mL}$  puromycin.

***Osteoclast differentiation assays***–Osteoclasts were generated from human blood CD14<sup>+</sup> or murine bone marrow CD11b<sup>+</sup> monocytes isolated magnetically (Miltenyi Biotec), and cultured in the presence of 25 ng/mL M-CSF and 100 ng/mL RANKL with or without Pep8 at 1-100 μM as described previously.<sup>(36)</sup> TRAP-positive multinucleated cells formed with ≥3 nuclei were considered as osteoclasts, manually counted and analyzed. IC<sub>50</sub> values for the dose-response experiments were calculated by linear extrapolation using the formula:  $IC_{50} = (50\% - Low_{Inh\%}) / (High_{Inh\%} - Low_{Inh\%}) \times (High_{Conc} - Low_{Conc}) + Low_{Conc}$ , where Low<sub>Inh%</sub>/High<sub>Inh%</sub> signify % inhibition directly below/above 50% inhibition, and Low<sub>Conc</sub>/High<sub>Conc</sub> are the corresponding concentrations of Pep8.

***Pit formation assay***–Osteoclast capacity for bone resorption was assessed by pit formation assay.<sup>(37;38)</sup> For this purpose, CD14-selected human osteoclast precursors (2×10<sup>5</sup> cells in 300 μL/well) were cultured on 5-mm-diameter dentin slices in 48-well culture plates in the presence of 30 ng/mL M-CSF. On day 3, cultures were supplemented with fresh medium containing M-CSF and RANKL (50 ng/mL) in the presence or absence of Pep8 (50, 100 and 300 μM). Medium and treatments were replaced every three days. At the end of the culture period on day 12, dentin slices were washed and adherent osteoclasts and mononuclear cells were removed manually. Resorption pits were observed by scanning electron microscopy (TM3000, Hitachi).

***RNA isolation and real-time PCR analysis***–Total RNA from CD14<sup>+</sup> cells treated in the presence or absence of Pep8 (50 μM) and/or hRANKL (100 ng/mL) was extracted using the Nucleospin RNA II kit (Macherey-Nagel) according to the manufacturer's instructions. First-strand cDNA was synthesized from 5 μg total RNA with ThermoScript™ RT (Invitrogen) and oligo(dT)

primers. Quantitative real-time PCR was carried out on a Chromo4™ System (Biorad) with a reaction mix containing 15-40 ng reverse-transcribed total RNA, 300 nM primers (see **Table S1** for primer sequences and PCR conditions) and 2×SYBR green buffer. GAPDH and B2M were used as reference genes for data normalization using the DDCT method, and relative target gene expression was calculated with the GenEx software (Biorad).<sup>(39;40)</sup>

**Western blot analysis**—RAW264.7 cells in culture were starved for 2 hours prior to treatment with Pep8 (50 μM) with or without hRANKL (100 ng/mL). Total cell lysates were obtained as described previously.<sup>(28)</sup> Separate cytoplasmic and nuclear protein fractions were obtained using the NE-PER Nuclear and Cytoplasmic Extraction Kit (Thermo Scientific). Proteins (40 μg) were run on SDS-PAGE and transferred to Immobilon-P membranes (Millipore), which were then incubated with antibodies (Cell Signalling) to Akt, phospho(p)-Akt, ERK 1/2, p-ERK 1/2, p38, p-p38, IκBα, p65 and p50 and visualized using the ECL reagent (Pierce). β-Actin, histone H3 and HDAC served as housekeeping proteins. HEK-RANK cells were pre-treated with Pep8 (50 μM) for 2 hours in serum-free medium before adding RANKL (5-50 ng/mL) and lysates were immunoblotted with p38/p-p38, as described above. For experiments with cycloheximide, cells were cultured in DMEM/FBS-1% over night and pre-treated with CHX (4 μg/mL) for 2 hours before treatment with RANKL (100 ng/mL) or Pep8 (200 μM) for 2 to 22 hours, respectively. RANK expression was analyzed by immunoblotting with anti-RANK/TNFRSF11A (R&D Systems).

**Murine model of osteoporosis**—Eight-week-old ovariectomized female C57BL6 and age-matched healthy mice were purchased from Janvier. Mice were housed under pathogen-free conditions at the Experimental Therapy Unit (University of Nantes, France). Animal care and

experimental protocols were approved by the French Ministry of Research and were done in accordance with the institutional guidelines of the French Ethical Committee and under the supervision of authorized investigators. After recovery from surgery for 7 days and acclimation, the mice were randomly divided into a treatment and a control group (n = 8 per group). Mice received daily subcutaneous injections of Pep8 (10 mg/kg) or vehicle. Non-ovariectomized mice were included as healthy controls. During the experimental period, the body weight of animals was monitored. After treatment for five weeks, mice were anesthetized with isoflurane and sacrificed by cervical disruption. Hind limbs and vertebrae were collected and stored at 4°C in 4% paraformaldehyde until further analysis. Internal organs were harvested, fixed in 4% PFA and paraffin-embedded for toxicity screening.

***Micro-CT analysis of bone samples***—Analysis of architectural variables of tibiae and vertebrae was performed using the high-resolution X-ray micro-CT system for small animal imaging SkyScan-1076 (at 50 kV and 200  $\mu$ A using a 0.5 mm aluminum filter and a detection pixel size of 18  $\mu$ m). Images were captured every 0.6° through 180° rotation. After scanning, the image data were transferred to a workstation and the proximal tibiae and the fourth lumbar vertebrae (L4) were rendered for 3D display and calculation of the structural indices<sup>(41)</sup> using the SkyScan analysis system. For trabecular bone parameters in tibiae, fifty slices (1 mm) at ~0.4  $\mu$ m distal to the growth plate were used for analysis. For the analysis of the L4 vertebrae, 120 slices (2.4 mm) were manually delineated within the vertebral body to avoid the inclusion of the superior and inferior endplates. The analysis involved the following bone measurements: bone volume fraction (BV/TV), trabecular number (TbN), trabecular thickness (TbTh) and trabecular spacing (TbSp).

**Bone histology and histomorphometry**—Left hind limbs and lumbar vertebrae fixed in 4% PFA were decalcified with 4.13% EDTA and 0.2% paraformaldehyde in phosphate buffered saline (PBS) for 96 hours using the KOS microwave histostation (Milestone) before embedding in paraffin. Serial sagittal sections of 5- $\mu$ m thickness were cut with a microtome (Leica Microsystems), mounted on glass slides and stained with Masson trichrome.<sup>(42)</sup> Histomorphometric analysis was conducted in the proximal epiphyseal regions of tibiae by tartrate-resistant acid phosphatase (TRAP) staining to identify osteoclasts, as described previously.<sup>(43)</sup> Slides stained for TRAP were analyzed using a digital slide scanner (NanoZoomer 2.0-RS, Hamamatsu). The number of osteoclasts was evaluated by manually counting on digital slides. TRAP-positive multinucleated cells attached to bone were scored as osteoclasts.

**Statistical Analysis**—Data were analyzed using GraphPad Prism version 4.0 software (GraphPad). One-way ANOVA followed by Dunnett’s multiple comparison test was applied to compare multiple treatment groups. *P* values < 0.05 were considered significant.

## RESULTS

### **In silico generation of novel peptide RANK antagonists**

To identify new inhibitors of the RANK/RANKL interaction, we created a library of random peptides of variable length (7 to 13 amino acids) which were filtered based on their 1D sequence using an in-house protocol to ensure their solubility in aqueous solutions. The remaining  $\sim 2.5 \times 10^4$  sequences were used to generate 3D peptide conformations, and the virtual peptides were screened for receptor binding against RANK (Supplemental Material, **Fig. S1**). The crystal

structure of the RANK–RANKL complex<sup>(21;22)</sup> was used as a template for modeling peptides in complex with RANK. Based on the structural changes in RANK upon RANKL binding, we defined a potential binding site for our peptides in the hinge region between two cysteine-rich domains on RANK, which is responsible for the conformational change upon RANKL association (**Fig. 1A**).<sup>(21)</sup> More precisely, we chose a binding groove for peptide docking starting between residues Arg112 and Lys148 on RANK with a narrow opening between Glu126 (a key residue for RANKL-binding and recognition) and Lys97 and extending downwards towards residues Arg129/Arg130 (**Fig. 1A**). Glu126 and Lys97 are held in place by two unique disulfide bonds formed between Cys125 and Cys127, and Cys93-Cys113 on RANK, respectively, leading to a constrained conformation in this area. Docking experiments with peptides were performed in this putative binding pocket on RANK. To this aim, we developed a two-step protocol to computationally predict binding affinities of peptide-RANK complexes. After an initial high-throughput screening of  $2.5 \times 10^4$  peptides, the most promising candidates were subjected to a refined calculation protocol for a better characterization of the most favorable RANK-peptide interactions (**Fig. S1**).

### **Biological screening of small peptides targeting RANK**

After the docking process, we evaluated experimentally the activity of the peptides with the most promising poses (~40) in an osteoclastogenesis assay. The respective activities of a representative panel of 11 peptides (see **Table S2** for peptide sequences) on human osteoclast formation are shown in **Figure 1B**. At a 50  $\mu$ M concentration several peptides showed a mild to weak inhibitory effect on osteoclastogenesis, while two peptides, Pep501 and Pep8, exhibited strong activity, similar to that of the RANKL-targeting control peptides, OP3-4<sup>(19)</sup> and

WP9QY<sup>(18)</sup>. Because of the higher solubility of Pep8 in aqueous solution and the promising docking results, we chose to continue our studies with Pep8.

Our model suggests that Pep8 binding to RANK occurs via two different binding mechanisms: competitive N-terminal binding (i.e. responsible for peptide activity) with residues Asn1-Val2-Leu3-Lys4-Leu5 blocking the access of RANKL to Lys97 and Glu126 on RANK, which are critical for RANKL binding;<sup>(19)</sup> and RANK-specific C-terminal binding of residues Cys6-Ser7-Gly8-Glu9 without RANKL interaction (i.e. conferring receptor affinity). **Figure 1C** shows the structure model of Pep8 fixed on RANK and the specific inter-molecular contacts made by the modeled peptide with key amino acids in the putative binding pocket of the protein (for a more detailed description of predicted molecular interactions between Pep8 and RANK, see **Fig. S2**).

We used surface plasmon resonance to evaluate experimentally the binding of Pep8 to RANK. Pep8 bound to immobilized RANK in a dose-dependent manner ( $K_d$   $10.5 \times 10^{-6}$  M,  $k_{on}$   $4.95 \times 10^2$   $M^{-1}s^{-1}$ ,  $k_{off}$   $5.20 \times 10^{-3}$   $s^{-1}$ ), confirming direct peptide-receptor interaction (**Fig. 1D**).

### **Pep8 inhibits RANKL-induced osteoclast formation and activity**

The functionality of Pep8 was further assessed in a dose-response experiment. Pep8 caused a dose-dependent decrease in the number of TRAP-positive multinucleated cells formed in CD14<sup>+</sup> monocyte cultures, with an  $IC_{50}$  of  $45.3 \pm 3.7$   $\mu M$  (**Fig. 2A,B**). Furthermore, we evaluated cross-species activity of Pep8 on the mouse receptor ortholog of RANKL (sharing 77% sequence identity) and found a similar decrease in murine CD11b<sup>+</sup> osteoclast numbers ( $IC_{50} = 33.8 \pm 6.3$ ) (**Fig. 2A,B**). By contrast, Pep8 alone in the absence of RANKL did not modulate osteoclast development, nor did treatment with Pep8 affect osteoblast differentiation of mesenchymal stem cells (**Fig. S3**). Pep8 also had an effect on osteoclastic markers cathepsin K (CathK) and TRAP

as well as nuclear factor of activated T cells c1 (NFATc1), which is expressed during osteoclast differentiation, markedly reducing mRNA levels at all time points studied which is consistent with its inhibitory effect on osteoclastogenesis (**Fig. 2C**). In addition, we also examined the effect of Pep8 on the resorptive activity of osteoclasts generated from CD14<sup>+</sup> precursors. We found that Pep8 at 100 and 300  $\mu$ M strongly reduced the RANKL-induced formation of resorption-pits on dentin slices (**Fig. 3**), which are indicative of osteoclast activity.

### **Pep8 inhibits RANKL-induced RANK signaling**

To explore pathways by which Pep8 regulates osteoclast biology (**Fig. S4**), we investigated the effect of the peptide on RANKL-induced activation of Akt, p38 and ERK in murine macrophage-like RAW264.7 cells. Pep8 inhibited RANKL-induced phosphorylation of Akt, p38 and ERK (**Fig. 4A**). Pep8 also affected NF- $\kappa$ B signaling by blocking the RANKL-induced degradation of I $\kappa$ B $\alpha$  and subsequent nuclear translocation of p50 and p65 (**Fig. 4B**), as shown by an increase in I $\kappa$ B $\alpha$  levels in the cytosol and a decrease in NF- $\kappa$ B p65 in the nuclear fraction of cells treated with Pep8. Levels of p50 were also slightly, but not statistically significantly decreased. By contrast, Pep8 had no effect on the expression levels of RelB (data not shown), indicating that Pep8 exerts its activity on osteoclast precursors by inhibiting the classical NF- $\kappa$ B pathway.

We confirmed the effect of Pep8 on RANK signaling in human embryonic kidney (HEK) 293 cells stably expressing RANK (**Fig. S5**). Pep8 strongly inhibited activation of p38 after stimulation with RANKL at 10 and 50 ng/mL (**Fig. 4C**). Surprisingly, there was only a slight and not statistically significant inhibition of p38 phosphorylation at 5 ng/mL RANKL (see also **Fig. S6**). The absence of an effect of Pep8 at very low concentrations of RANKL may be explained by a cooperative binding mode in which the receptor affinity for the ligand depends on the

amount of ligand(s) bound to the receptor chains. In contrast to a linear binding mode where increasing ligand concentrations result in a linear recruitment/activation of the receptor, cooperative binding is characterized by a non-linear relationship between the number of receptor binding sites occupied by the ligand and the ligand concentration.<sup>(44)</sup> In our model, increasing RANKL concentrations may increase the binding affinity of Pep8 to RANK by substantially modifying the stoichiometric conformation of RANK receptor chains and/or their ability to form trimeric receptor complexes. This mechanism of cooperative receptor activation may be further exacerbated by the high receptor levels present in this cell model. Similar experiments carried out by us and others with different RANK-expressing cancer cell lines required high concentrations of RANKL (0.1 - 2.5  $\mu\text{g}/\text{mL}$ ) in order to activate downstream signaling.<sup>(6;45)</sup>

In addition, we also studied receptor half-life in this model. Pep8 induced receptor degradation in HEK-RANK cells over time when de novo protein synthesis was blocked, albeit to a somewhat lesser extent than what was observed with RANKL (**Fig. 4D**), which strongly supports our in silico prediction that Pep8 specifically binds to membrane RANK.

### **Pep8 protects mice against ovariectomy-induced bone loss**

Given Pep8's ability to inhibit RANKL-induced osteoclast differentiation and signaling in vitro, we asked whether Pep8 might prevent RANKL-dependent bone loss in an ovariectomized (OVX) mouse model.<sup>(46;47)</sup> Animals received daily subcutaneous injections of 10 mg/kg Pep8 over a period of 35 days. The peptide dosage was chosen based on previous murine studies using RANKL-targeting peptides.<sup>(18;19;48)</sup> Pep8 attenuated bone loss in OVX mice compared to vehicle-treated controls (**Fig. 5** and **Table 1**), as demonstrated by a significant increase in structural parameters, including trabecular bone volume (BV/TV, 93%), trabecular thickness (TbTh, 14%),

and trabecular number (TbN, 33%) with a decrease in trabecular separation (TbS, 20%) (all  $p < 0.01$ ). Similar results were obtained in lumbar vertebrae (**Fig. 5** and **Table 1**).

Histological analysis of the proximal tibiae from the respective groups revealed a marked increase in trabecular bone tissue in Pep8-treated mice, as well as a significant reduction of the number of TRAP-positive osteoclasts in tibiae (NOV,  $33.5 \pm 2.3$  and OVX,  $33.9 \pm 4.4$  versus Pep8,  $22.7 \pm 2.4$  osteoclasts/mm of bone perimeter;  $p < 0.01$ ) (**Fig. 5**), demonstrating an inhibition of osteoclast formation in vivo. Pep8 was well tolerated without any sign of overt toxicity at the tested dose, apart from transient hair loss close to the injection site which was observed in 7 out of 8 mice in the treatment group (**Fig. S7**). A histological evaluation of major organs showed no evidence of treatment-related organ toxicity (**Fig. S7**). Overall, these results provide evidence that Pep8 is a promising new agent for the treatment of postmenopausal bone loss.

### **Highlighting a core motif responsible for receptor binding**

To further understand the mechanism of action of Pep8, we performed one- and two-dimensional saturation transfer difference (STD) NMR experiments which allow the determination of the binding epitope of a peptide by measuring progressive saturation transfers from the protein to the ligand protons upon receptor binding.<sup>(49)</sup> To determine the ligand protons that are closer to the receptor upon binding, a spectrum in which the protein was selectively saturated is recorded, and the saturation transfer difference between a spectrum with saturation and one recorded without protein saturation can be quantified and constitutes an indication of binding. Only the signals of the protons that are in close contact to the protein and receive magnetization transfer will appear

in the difference spectrum and from those, the ones that are closer to the protein will have more intense signals, owing to a more efficient saturation transfer.

STD NMR spectra of RANK with increasing concentrations of Pep8 were recorded and peak intensities for all visible amide (NH) protons of the peptide were calculated. The 1D spectra of Pep8 bound to RANK differed significantly from that of the unbound peptide, in proportion to the amount of peptide added to the sample (**Fig. 6A**). To define the peptide residues which are critical for protein-binding we used a combination of transferred NOE (Nuclear Overhauser Effect) and STD experiments.<sup>(50)</sup> We observed the strongest STD signals (100%) for the NH protons of residues Leu3-Lys4-Leu5, demonstrating closest proximity of this motif to the protein surface (**Fig. 6B**). Residues Cys6-Ser7 and Gly8-Glu9 received strong (60%) and medium (40%) transfers of saturation, respectively. Residues Asn1 and Val2 were not visible in the spectrum, which is typical for this type of experiment; however, both terminal NH<sub>2</sub> protons of Asn1 were detected with low STD signals (**Fig. 6B**). Our STD results thus highlight the binding of a continuous core motif Leu3-Lys4-Leu5-Cys6-Ser7 (LKLCS) to the receptor, revealing a key role for these residues in abrogating ligand-binding. By contrast, no comparable binding motif could be defined for *in silico* binding to other members of the TNF-R family (**Fig. S8**), which further reinforces the notion of receptor-specificity of Pep8.

### **Creation of a novel series of effective RANK antagonists**

We next created a series of peptides derived from the sequence of Pep8 sharing  $\geq 80\%$  sequence identity (see **Table S3** for a full rationale of peptide modifications) with the aim to (i) further evaluate the individual contribution of each residue to receptor-binding and, and (ii) improve the inhibitory activity.

We first created peptides carrying modifications in the terminal regions of the peptide while maintaining an intact core LKLCS. As expected, most of these peptides showed an activity similar to that of Pep8 (**Fig. 6C**) as long as the peptide length was not affected, confirming a key role for these residues. The core 5-mer by itself (Pep822) without surrounding residues showed no in vitro activity which can be explained by its short length. Molecular docking also predicted an alternative binding mode in which the side chain of Lys4 is pointed towards RANK-Glu126 instead of adopting the preferred head-to-tail orientation with Lys97 (**Fig. S9**). Furthermore, an exchange of N- and C-terminal residues (Pep813) lead to an upside-down orientation of the peptide (which had almost no consequence for peptide activity), revealing the nearly palindromic nature of the sequence and demonstrating that the peptide orientation is determined by its surrounding amino acids (**Fig. 6C** and **Fig. S9**).

We also introduced specific modifications to enhance peptide affinity (i.e. RANK-binding); however, this lead to a mild decrease in activity (**Fig. 6C**). To further enhance peptide activity, we created derivatives with specific modifications in the core motif. We demonstrated that although the position of the peptide in the binding groove and the hydrogen bond network formed between these residues and the receptor are important, specific substitutions can be introduced that can compensate for the loss of interactions due to the nature of the residue or the displacement of the peptide around Glu126, the key residue for receptor-ligand binding (**Fig. 6C** and **Fig. S9**). Taken together, these results demonstrate that our method is able to reliably predict in vitro activities of peptides and their derivatives, and is a valuable tool for the design and improvement of novel peptide inhibitors.

## DISCUSSION

Over the past decade, new therapeutic options for the treatment of bone disease and skeletal-related events (SRE) have emerged, including bisphosphonates<sup>(51;52)</sup> and antibody-driven biotherapies such as the RANKL-targeting antibody denosumab.<sup>(53)</sup> However, important limitations remain including the high cost associated with the manufacturing and/or purification process and the risk of side effects such as rashes, hypocalcaemia or renal toxicity.<sup>(16;17)</sup> There remains therefore a need for effective, affordable therapies with fewer side effects that address the causes of the disease.

A promising therapeutic alternative is the use of inhibitory peptides or peptidomimetics of protein-protein interaction, which has been applied to various members of the TNF receptor family, such as the OPG mimetic OP3-4 or the RANK mimetic L3-3.<sup>(18-23;54)</sup> However, the most effective inhibitors published to date were active against the ligand rather than the receptor.

We have developed a new strategy to inhibit RANK activation by blocking a receptor conformation to reduce its conformational entropy. We defined a potential binding region for our peptides in the hinge region of the receptor which undergoes a conformational change during ligand-binding. Contrary to the approaches presented so far, we did not use the amino acids from the RANK/RANKL interface as starting templates, but instead generated an in-house library of soluble peptides and screened for peptide activity by performing docking experiments on the receptor. Such high-throughput virtual screening is an important tool in the drug discovery process and is often successful in identifying competitive peptides; however, their further experimental validation is often limited or even prevented by a low aqueous solubility of the peptides and may therefore require additional modifications. To address this problem, we have developed an original approach that guarantees peptide solubility while also drastically reducing the conformational space to explore. Existing tools for the prediction of peptide solubility, which are mostly based on machine learning approaches on protein structures, are unsuitable for small

peptides, since the 3D conformation of short polypeptides ( $\leq 15$  amino acids) is more likely to be unstructured.<sup>(55)</sup> By contrast, our approach is rule-based to exclude common peptide compositions known to prevent good solubilization in water and allows a dramatic reduction of the original peptide collection to only 5-20% of its initial size and may provide a first step towards a more general set of rules for peptide solubility, useful for pre-filtering a peptide library.

After the virtual screening process, we evaluated experimentally the activity of the most promising poses, since the post-docking scoring methods were not sufficient to discriminate clearly amongst them, as is often the case in blind virtual screening evaluations.<sup>(56)</sup> We successfully tested the most promising peptide, Pep8, derived from this approach for its inhibitory activity in vitro and on bone loss in a mouse osteoporosis model. Pep8 was well tolerated in vivo without any signs of treatment-related toxicity. The minor side effect of transient hair loss observed in the Pep8-treated group, which can be explained by the involvement of RANK/RANKL in the hair renewal process,<sup>(57)</sup> was not observed in mice treated with a lower dose (5 mg/kg/d) of Pep8, although the bone-sparing effect at this dose was also less pronounced (**Fig. S10**), indicating a dose-dependent mechanism. Overall, our data thus provide evidence that Pep8 is a promising new agent for the treatment of RANKL-mediated bone loss.

Receptor binding and specificity of Pep8 was further validated using biological as well as biophysical experiments, confirming in silico predictions that Pep8 specifically binds to membrane RANK, while no receptor-binding sites could be defined for other members of the receptor family. Using STD NMR spectroscopy, we highlighted a key role for the central peptide motif LKLCS in blocking the receptor-ligand interaction. Following the classical hit-to-lead

strategy,<sup>(58)</sup> we also determined *in silico* the individual contribution of each residue to the binding of Pep8 to RANK, which led to the generation of a series of 24 RANK antagonists derived from the original sequence and provided valuable insight into the mechanism of action of Pep8, which can be exploited for further peptide refinement to maximize inhibitory activity. Furthermore, our approach should be easily adaptable to other genetic variants of RANK<sup>(59)</sup> or to specifically target other members of the TNF-R family while avoiding cross-reactivity.

For example, several disease-associated mutations have been identified so far in the extracellular domain of RANK where Pep8 binds to the receptor.<sup>(60;61)</sup> However, most identified mutations are located outside of the RANKL-binding interface with no consequences for peptide binding. By contrast, mutations in residues that are involved in RANKL-binding, such as residues R128 and R129, may lead to a modification of the receptor-peptide interaction, with possible consequences on peptide activity. To counter a loss of activity, specific peptide sequence mutations may be introduced to restore full peptide-binding to RANK, provided that the structural integrity of the receptor is maintained in the mutant.<sup>(62)</sup> However, some mutations may induce structural changes in the receptor such as the mutation of R129 to a cysteine, which may disturb locally the A/B fold highly conserved in members of the TNF family<sup>(63)</sup> via the formation of alternative disulfide bridges. Such potential conformational changes could modulate the affinity of the receptor to its ligand, leading to a total loss of peptide binding, and may also explain why patients carrying the 128/129 mutations are susceptible to develop the osteoclast-poor osteopetrosis phenotype.<sup>(60)</sup> With regard to peptide design, it is essential to evaluate experimentally the consequences of these mutations on the receptor conformation prior to the design of novel inhibitory peptides.

A remaining concern for the use of therapeutic peptides is their short *in vivo* activity due to poor bioavailability and rapid renal clearance.<sup>(64)</sup> However, recent advances in novel systemic or local drug delivery systems have provided options for more effective drug administration.<sup>(65)</sup> Further

experimental validation is required to confirm the druglikeness of our peptides in preclinical studies; however, our results may constitute a tangible step toward the use of RANK antagonists in bone resorptive disease, alone or in conjunction with existing therapies.

## **DISCLOSURES**

All the authors state that they have no conflict of interest.

## **ACKNOWLEDGMENTS**

This research article is dedicated to the memory of our dear colleague Marc Padrines, who left us too early. The authors thank Mike Maillason from the “Plate-forme Impact-Interactions Moléculaires Puces Activités/Biogenouest, SFR Bonamy, University of Nantes” for the surface plasmon resonance experiments. This work was supported by the Fond Unique Interministeriel n°08 90 6214 (GELTOP project). K. Ando received a postdoctoral fellowship from the Region des Pays de La Loire (France).

Authors' roles: Conception and coordination of the project: DH. Study design: ST and VS. In silico and biophysical studies: ST and GB. In vitro and in vivo studies: VS, SH, MB, MFH, CC and KA. Data analysis and interpretation: VS, ST, SH and GB. Writing and critical review of manuscript: VS and ST. All authors read and approved the final version of the manuscript. VS and ST take responsibility for the integrity of the data analysis.

## **REFERENCES**

1. Zaidi M, Skeletal remodeling in health and disease. *Nat Med.* 2007;13(7):791–801.
2. Aubin JE, Triffitt JT. *Principles of Bone Biology* (2<sup>nd</sup> ed.) 2002, pp 59–81. Academic Press, San Diego.

3. Anderson DM, Maraskovsky E, Billingsley WL, Dougall WC, Tometsko ME, Roux ER, Teepe MC, DuBose RF, Cosman D, Galibert L. A homologue of the TNF receptor and its ligand enhance T-cell growth and dendritic-cell function. *Nature*. 1997;390(6656):175–9.
4. Boyle WJ, Simonet WS, Lacey DL. Osteoclast differentiation and activation. *Nature*. 2003;423:337–42.
5. Simonet W, Lacey D, Dunstan C, Kelley M, Chang M-S, Lüthy R, Nguyen H, Wooden S, Bennett L, Boone T, Shimamoto G, DeRose M, Elliott R, Colombero A, Tan HL, Trail G, Sullivan J, Davy E, Bucay N, Renshaw-Gegg L, Hughes TM, Hill D, Pattison W, Campbell P, Sander S, Van G, Tarpley J, Derby P, Lee R, Boyle WJ. Osteoprotegerin: A novel secreted protein involved in the regulation of bone density. *Cell*. 1997;89(2):309–19.
6. Jones DH, Nakashima T, Sanchez OH, Kozieradzki I, Komarova SV, Sarosi I, Morony S, Rubin E, Sarao R, Hojilla CV, Komnenovic V, Kong Y-Y, Schreiber M, Dixon SJ, Sims SM, Khokha R, Wada T, Penninger JM. Regulation of cancer cell migration and bone metastasis by RANKL. *Nature*. 2006;440(7084):692–6.
7. Heymann D, Fortun Y, Rédini F, Padrines M. Osteolytic bone diseases: physiological analogues of bone resorption effectors as alternative therapeutic tools. *Drug Discov Today*. 2005;10(4):242–7.
8. Jules J, Ashley JW, Feng X. Selective targeting of RANK signaling pathways as new therapeutic strategies for osteoporosis. *Expert Opin Ther Targets*. 2010;14(9):923–34.
9. Feeley BT, Liu NQ, Conduah AH, Krenek L, Roth K, Dougall WC, Huard J, Dubinett S, Lieberman JR. Mixed metastatic lung cancer lesions in bone are inhibited by Noggin overexpression and Rank:Fc administration. *J Bone Miner Res*. 2006;21(10):1571–80.
10. Lamoureux F, Picarda G, Rousseau J, Gourden C, Battaglia S, Charrier C, Pitard B, Heymann D, Rédini F. Therapeutic efficacy of soluble receptor activator of nuclear factor-kappa B-Fc delivered by nonviral gene transfer in a mouse model of osteolytic osteosarcoma. *Mol Cancer Ther*. 2008;7(10):3389–98.
11. Body J-J, Greipp P, Coleman RE, Facon T, Geurs F, Femand J-P, Harousseau J-L, Lipton A, Mariette X, Williams CD, Nakanishi A, Holloway D, Martin SW, Dunstan CR, Bekker PJ. A Phase I study of AMGN-0007, a recombinant osteoprotegerin construct, in patients with multiple myeloma or breast carcinoma related bone metastases. *Cancer*. 2003;97(Suppl. 3):887–92.
12. Lamoureux F, Picarda G, Garrigue-Antar L, Baud'huin M, Trichet V, Vidal A, Miot-Noirault E, Pitard B, Heymann D, Rédini F. Glycosaminoglycans as potential regulators of osteoprotegerin therapeutic activity in osteosarcoma. *Cancer Res*. 2009;69(2):526–36.
13. Rousseau J, Escriou V, Lamoureux F, Brion R, Chesneau J, Battaglia S, Amiaud J, Scherman D, Heymann D, Rédini F, Trichet V. Formulated siRNAs targeting Rankl prevent osteolysis and enhance chemotherapeutic response in osteosarcoma models. *J Bone Miner Res*. 2011;26(10):2452–62.
14. Cohen SB, Dore RK, Lane NE, Ory PA, Peterfy CG, Sharp JT, van der Heijde D, Zhou L, Tsuji W, Newmark R. Denosumab treatment effects on structural damage, bone mineral density, and bone turnover in rheumatoid arthritis: A twelve-month, multicenter, randomized, double-blind, placebo-controlled, phase II clinical trial. *Arthritis Rheum*. 2008;58:1299–309.

15. Heymann D. Anti-RANKL therapy for bone tumours: Basic, pre-clinical and clinical evidences. *J Bone Oncol.* 2012;1:2–11.
16. Xie J, Namjoshi M, Wu EQ, Parikh K, Diener M, Yu AP, Guo A, Culver KW. Economic evaluation of denosumab compared with zoledronic acid in hormone-refractory prostate cancer patients with bone metastases. *J Manag Care Pharm.* 2011;17(8):621–43.
17. Wada T, Nakashima T, Hiroshi N, Penninger JM. RANKL-RANK signaling in osteoclastogenesis and bone disease. *Trends Mol Med.* 2006;12(1):17–25.
18. Aoki K, Saito H, Itzstein C, Ishiguro M, Shibata T, Blanque R, Mian AH, Takahashi M, Suzuki Y, Yoshimatsu M, Yamaguchi A, Deprez P, Mollat P, Murali R, Ohya K, Horne WC, Baron R. A TNF receptor loop peptide mimic blocks RANK ligand-induced signaling, bone resorption, and bone loss. *J Clin Invest.* 2006; 116(6):1525–34.
19. Cheng X, Kinoshita M, Takami M, Choi Y, Zhang H, Murali R. Disabling of receptor activator of nuclear factor- $\kappa$ B (RANK) receptor complex by novel osteoprotegerin-like peptidomimetics restores bone loss in vivo. *J Biol Chem.* 2004;279(9):8269–77.
20. Hasegawa A, Cheng X, Kajino K, Berezov A, Murata K, Nakayama T, Yagita H, Murali R, Greene MI. Fas-disabling small exocyclic peptide mimetics limit apoptosis by an unexpected mechanism. *Proc Natl Acad Sci USA.* 2004;101(17):6599–604.
21. Liu C, Walter TS, Huang P, Zhang S, Zhu X, Wu Y, Wedderburn LR, Tang P, Owens RJ, Stuart DI, Ren J, Gao B. Structural and functional insights of RANKL-RANK interaction and signaling. *J Immunol.* 2010;184(12):6910–19.
22. Ta HM, Nguyen GTT, Jin HM, Choi J, Park H, Kim N, Hwang H-Y, Kim KK. Structure-based development of a receptor activator of nuclear factor- $\kappa$ B ligand (RANKL) inhibitor peptide and molecular basis for osteopetrosis. *Proc Natl Acad Sci USA.* 2010;107(47):20281–6.
23. Kajiwara K, Saito A, Ogata S, Tanihara M. Synthetic peptides corresponding to ligand-binding region of death receptors, DR5, Fas, and TNFR, specifically inhibit cell death mediated by the death ligands, respectively. *Biochim Biophys Acta.* 2004;1699:131–7.
24. Theoleyre S, Wittrant Y, Tat SK, Fortun Y, R dini F, Heymann D. The molecular triad OPG/RANK/RANKL: involvement in the orchestration of pathophysiological bone remodeling. *Cytokine Growth Factor Rev.* 2004;15(6):457–75.
25. Lien S, Lowman HB. Therapeutic peptides. *Trends Biotechnol.* 2003;21(12):556–62.
26. Brooks BR, Bruccoleri RE, Olafson BD, States DJ, Swaminathan S, Karplus M. CHARMM: A program for macromolecular energy, minimization, and dynamics calculations. *J Comp Chem.* 1983;4(2):187–217.
27. Wu G, Robertson DH, III CLB, Vieth M. Detailed analysis of grid-based molecular docking: A case study of CDOCKER - A CHARMM-based MD docking algorithm. *J Comp Chem.* 2003;24(13):1549–62.
28. Baudhuin M, Duplomb L, Teletchea S, Charrier C, Maillason M, Fouassier M, Heymann D. Factor VIII/Von Willebrand factor complex inhibits osteoclastogenesis and controls cell survival. *J Biol Chem.* 2009;284(46):31704–13.

29. States DJ, Haberkorn RA, Ruben DJ. A two-dimensional nuclear Overhauser experiment with pure absorption phase in four quadrants. *J Magn Reson.* 1982;48:286–92.
30. Piotto M, Saudek V, Sklenár V. Gradient-tailored excitation for single-quantum NMR spectroscopy of aqueous solutions. *J Biomol NMR.* 1992;2(6):661–5.
31. Hwang TL, Shaka AJ. Water suppression that works. Excitation sculpting using arbitrary wave-forms and pulsed-field gradients. *J Magn Reson. Ser A.* 1995;112:275–9.
32. Bax A, Davis DG. MLEV-17-based two-dimensional homonuclear magnetization transfer spectroscopy. *J Magn Res.* 1985;65:355–60.
33. Pons J, Evrard-Todeschi N, Bertho G, Gharbi-Benarous J, Sonois V, Benarous R, Girault J-P. Structural studies on 24P-IkappaBalpha peptide derived from a human IkappaB-alpha protein related to the inhibition of the activity of the transcription factor NF-kappaB. *Biochemistry.* 2007;46:2958–72.
34. Xia Y, Zhu Q, Jun K-Y, Wang J, Gao X. Clean STD-NMR spectrum for improved detection of ligand-protein interactions at low concentration of protein. *Magn Reson Chem.* 2010;48:918–24.
35. Cutting B, Shelke SV, Dragic Z, Wagner B, Gathje H, Kelm S, Ernst B. Sensitivity enhancement in saturation transfer difference (STD) experiments through optimized excitation schemes. *Magn Reson Chem.* 2007;45:720–4.
36. Baud'Huin M, Renault R, Charrier C, Riet A, Moreau A, Brion R, Gouin F, Duplomb L, Heymann D. Interleukin-34 is expressed by giant cell tumours of bone and plays a key role in RANKL-induced osteoclastogenesis. *J Pathol.* 2010;221(1):77–86.
37. Boyde A, Ali NN, Jones SJ. Resorption of dentine by isolated osteoclasts in vitro. *Brit Dent J.* 1984;156:216–220.
38. Baud'huin M, Charrier C, Bougras G, Brion R, Lezot F, Padrines M, Heymann D. Proteoglycans and osteolysis. *Methods Mol Biol.* 2012;836:323-37.
39. Pfaffl MW. A new mathematical model for relative quantification in real-time RT-PCR. *Nucleic Acids Res.* 2001;29(9):e45.
40. Vandesompele J, De Preter K, Pattyn F, Poppe B, Van Roy N, De Paepe A, Speleman F. Accurate normalization of real-time quantitative RT-PCR data by geometric averaging of multiple internal control genes. *Genome Biol.* 2002;3(7):RESEARCH0034.
41. Parfitt AM, Drezner MK, Glorieux FH, Kanis JA, Malluche H, Meunier PJ, Ott SM, Recker RR. Bone histomorphometry: standardization of nomenclature, symbols, and units. Report of the asbmr histomorphometry nomenclature committee. *J Bone Miner Res.* 1987;2(6):595–610.
42. Heymann D, Ory B, Blanchard F, Heymann M-F, Coipeau P, Charrier C, Couillaud S, Thiéry JP, Gouin F, Rédini F. Enhanced tumor regression and tissue repair when zoledronic acid is combined with ifosfamide in rat osteosarcoma. *Bone.* 2005;37(1):74–86.
43. Lamoureux F, Picarda G, Garrigue-Antar L, Baud'huin M, Trichet V, Vidal A, Miot-Noirault E, Pitard B, Heymann D, Rédini F. Glycosaminoglycans as potential regulators of osteoprotegerin therapeutic activity in osteosarcoma. *Cancer Res.* 2009;69(2):526–36.

44. Edelstein SJ, Le Novère N. Cooperativity of allosteric receptors. *J Mol Biol.* 2013;425(9):1424–32.
45. Mori K, Le Goff B, Charrier C, Battaglia S, Heymann D, Rédini F. DU145 human prostate cancer cells express functional receptor activator of NFkappaB: new insights in the prostate cancer bone metastasis process. *Bone.* 2007;40(4):981–90.
46. Cenci S, Weitzmann MN, Roggia C, Namba N, Novack D, Woodring J, Pacifici R. Estrogen deficiency induces bone loss by enhancing T-cell production of TNF- $\alpha$ . *J Clin Invest.* 2000;106(10):1229–37.
47. Roggia C, Gao Y, Cenci S, Weitzmann MN, Toraldo G, Isaia G, Pacifici R. Up-regulation of TNF-producing T cells in the bone marrow: a key mechanism by which estrogen deficiency induces bone loss in vivo. *Proc Natl Acad Sci USA.* 2001;98(24):13960–5.
48. Heath DJ, Vanderkerken K, Cheng X, Gallagher O, Prideaux M, Murali R, Croucher P. An osteoprotegerin-like peptidomimetic inhibits osteoclastic bone resorption and osteolytic bone disease in myeloma. *Cancer Res.* 2007;67:202–8.
49. Pons J, Tanchou V, Girault J-P, Bertho G, Evrard-Todeschi N. NMR applications for identifying  $\beta$ -TrCP protein-ligand interactions. *Mini Rev Med Chem.* 2011;11(4):283–97.
50. Kumar A, Wagner G, Ernst RR, Wuethrich K. Buildup rates of the nuclear Overhauser effect measured by two-dimensional proton magnetic resonance spectroscopy: implications for studies of protein conformation. *J Am Chem Soc.* 1981;103:3654–8.
51. Heymann D, Ory B, Gouin F, Green JR, Rédini F. Bisphosphonates: new therapeutic agents for the treatment of bone tumors. *Trends Mol Med.* 2004;10(7):337–43.
52. Stresing V, Daubiné F, Benzaid I, Mönkkönen H, Clézardin P. Bisphosphonates in cancer therapy. *Cancer Lett.* 2007;257(1):16–35.
53. Kostenuik PJ, Nguyen HQ, McCabe J, Warmington KS, Kurahara C, Sun N, Chen C, Li L, Cattley RC, Van G, Scully S, Elliott R, Grisanti M, Morony S, Tan HL, Asuncion F, Li X, Ominsky MS, Stolina M, Dwyer D, Dougall WC, Hawkins N, Boyle WJ, Simonet WS, Sullivan JK. Denosumab, a fully human monoclonal antibody to RANKL, inhibits bone resorption and increases BMD in knock-in mice that express chimeric (murine/human) RANKL. *J Bone Miner Res.* 2009;24(2):182–95.
54. Takasaki W, Kajino Y, Kajino K, Murali R, Greene MI. Structure-based design and characterization of exocyclic peptidomimetics that inhibit TNF[ $\alpha$ ] binding to its receptor. *Nat Biotechnol.* 1997;15(12):1266–70.
55. Vanhee P, Stricher F, Baeten L, Verschueren E, Lenaerts T, Serrano L, Rousseau F, Schymkowitz J. Protein-peptide interactions adopt the same structural motifs as monomeric protein folds. *Structure.* 2009;17(8):1128–36.
56. Fleishman SJ, Whitehead TA, Strauch E-M, Corn JE, Qin S, Zhou H-X, Mitchell JC, Demerdash ONA, Takeda-Shitaka M, Terashi G, Moal IH, Li X, Bates PA, Zacharias M, Park H, Ko J, Lee H, Seok C, Bourquard T, Bernauer J, Poupon A, Azé J, Soner S, Ovali SK, Ozbek P, Tal NB, Haliloglu T, Hwang H, Vreven T, Pierce BG, Weng Z, Pérez-Cano L, Pons C, Fernández-Recio J, Jiang F, Yang F, Gong X, Cao L, Xu X, Liu B, Wang P, Li C,

- Wang C, Robert CH, Guharoy M, Liu S, Huang Y, Li L, Guo D, Chen Y, Xiao Y, London N, Itzhaki Z, Schueler-Furman O, Inbar Y, Potapov V, Cohen M, Schreiber G, Tsuchiya Y, Kanamori E, Standley DM, Nakamura H, Kinoshita K, Driggers CM, Hall RG, Morgan JL, Hsu VL, Zhan J, Yang Y, Zhou Y, Kastiris PL, Bonvin AM, Zhang W, Camacho CJ, Kilambi, A Sircar, JJ Gray, M Ohue, N Uchikoga, Y Matsuzaki, T Ishida, Y Akiyama, R Khashan KP, Bush S, Fouches D, Tropsha A, Esquivel-Rodríguez J, Kihara D, Stranges PB, Jacak R, Kuhlman B, Huang SY, Zou X, Wodak SJ, Janin J, Baker D. Community-wide assessment of protein-interface modeling suggests improvements to design methodology. *J Mol Biol.* 2011;414(2):289–302.
57. Duheron V, Hess E, Duval M, Decossas M, Castaneda B, Klöpffer JE, Amoasii L, Barbaroux J-B, Williams IR, Yagita H, Penninger J, Choi Y, Lézot F, Groves R, Paus R, Mueller CG. Receptor activator of NF- $\kappa$ B (RANK) stimulates the proliferation of epithelial cells of the epidermo-pilosebaceous unit. *Proc Natl Acad Sci USA.* 2011;108(3):5342–7.
  58. Bleicher KH, Böhm H-J, Müller K, Alanine AI. Hit and lead generation: beyond high-throughput screening. *Nat Rev Drug Discov.* 2003;2(5):369–78.
  59. Pangrazio A, Cassani B, Guerrini MM, Crockett JC, Marrella V, Zammataro L, Strina D, Schulz A, Schlack C, Kornak U, Mellis DJ, Duthie A, Helfrich MH, Durandy A, Moshous D, Vellodi A, Chiesa R, Veys P, Iacono N, Vezzoni P, Fischer A, Villa A, Sobacchi C. RANK-dependent autosomal recessive osteopetrosis: Characterization of five new cases with novel mutations. *J Bone Miner Res.* 2012;27(2): 342–51.
  60. Guerrini MM, Sobacchi C, Cassani B, Abinun M, Kilic SS, Pangrazio A, Moratto D, Mazzolari E, Clayton-Smith J, Orchard P, Coxon FP, Helfrich MH, Crockett JC, Mellis D, Vellodi A, Tezcan I, Notarangelo LD, Rogers MJ, Vezzoni P, Villa A, Frattini A. Human osteoclast-poor osteopetrosis with hypogammaglobulinemia due to TNFRSF11A (RANK) mutations. *Am J Hum Genet.* 2008;83(1):64–76.
  61. Sherry ST, Ward MH, Kholodov M, Baker J, Phan L, Smigielski EM, Sirotkin K. dbSNP: the NCBI database of genetic variation. *Nucleic Acids Res.* 2001;29(1):308–11
  62. Weinkam P, Chen YC, Pons J, Sali A. Impact of mutations on the allosteric conformational equilibrium. *J Mol Biol.* 2013;425(3):647–61.
  63. Naismith JH, Sprang SR. Modularity in the TNF-receptor family. *Trends Biochem Sci.* 1998;23(2):74–9.
  64. McGregor DP. Discovering and improving novel peptide therapeutics. *Curr Opin Pharmacol.* 2008;8(5):616–9.
  65. Aoki K, Alles N, Soysa N, Ohya K. Peptide-based delivery to bone. *Adv Drug Delivery Rev.* 2012;64(12):1220–38.

## FIGURE LEGENDS

**Fig. 1.** Structure-based design of peptide RANK antagonists. **(A)** Structure of the RANK/RANKL complex with amino acids (AAs) colored according to interpolated charge (blue, positive; red, negative; white, neutral and/or hydrophobic). (i) The RANK/RANKL interface (shown are two monomers) is discontinuous with two binding zones forming a cavity between cytokine and receptor. (ii,iii) Main AAs defining the edges of the putative peptide binding groove in the hinge region on RANK. (iv) 3D model of a peptide-RANK complex. **(B)** Screening of novel peptides for osteoclast differentiation. TRAP<sup>+</sup> multinucleated cells (MNCs) formed in cultures of CD14<sup>+</sup> monocytes incubated in the presence of M-CSF/RANKL and a peptide (50  $\mu$ M) are counted. OPG served as positive control. Results are expressed as percentage of TRAP<sup>+</sup> cells in cultures without a peptide and are the means  $\pm$  SD of three experiments done in triplicate. **(C)** Ball-and-stick representation of a 3D conformation of Pep8 (9-mer sequence NVLKLCSGE) in complex with RANK from molecular modeling. Interacting AAs from RANK making contact with the modeled Pep8 are shown as grey-blue spheres. Key AAs E126 and K97 are marked in red. **(D)** Surface plasmon resonance sensorgrams showing the formation and dissociation of the Pep8:RANK complex (injection spikes removed). Samples of Pep8 at different concentrations were injected over immobilized RANK.

**Fig. 2.** Inhibitory effect of Pep8 on RANKL-induced osteoclastogenesis. **(A)** Activity of Pep8 on osteoclast formation in human CD14<sup>+</sup> and murine CD11b<sup>+</sup> monocytes. Representative microscopic images of TRAP<sup>+</sup> MNCs at different concentrations of Pep8 are shown. **(B)** The percentage of TRAP<sup>+</sup> cells was measured. The values represent means  $\pm$  SD of at least three independent experiments carried out in triplicate. \*\* $p < 0.01$  and \* $p < 0.05$ . **(C)** Relative expression of osteoclast-specific genes CathK and TRAP and NFATc1 in CD14<sup>+</sup> cells treated

with Pep8 in the presence or absence of RANKL (for 3, 6 and 9 days). Expression levels were normalized to GAPDH and B2M and the level of undifferentiated cells (-RANKL) at day 3 was set to 1. Graphs show the results of representative experiments run in triplicate. Values represent means  $\pm$  SD of technical triplicates. **\*\* $p < 0.01$  and \* $p < 0.05$ .**

**Fig. 3.** Effect of Pep8 on osteoclast activity. The effect of Pep8 on the formation of resorption pits on dentine slices (50 $\times$  original magnification) was assessed in CD14<sup>+</sup> cell cultures incubated with RANKL (50 ng/mL) and Pep8 (50, 100 or 300  $\mu$ M, as indicated). Dentin slices cultured with RANKL only served as controls. Pep8 strongly suppressed RANKL-stimulated bone resorption at 100 and 300  $\mu$ M. Representative images of pit formation on dentin slices from two independent experiments are shown. Scale bars, 500  $\mu$ m.

**Fig. 4.** Effect of Pep8 on RANK signaling. **(A)** Inhibition of activation of Akt, p38 and ERK by Pep8 (50  $\mu$ M) was assessed as inhibition of phosphorylation (p-) in RAW264.7 cells. **(B)** NF- $\kappa$ B distribution in the presence or absence of Pep8. **Expression of inhibitor protein I $\kappa$ B $\alpha$  and NF- $\kappa$ B proteins p65 and p50 were analyzed in the cytoplasmic (CF) or nuclear fractions (NF).** **(C)** Effect of Pep8 (100  $\mu$ M) on p38 activation in HEK293 cells overexpressing RANK (HEK-RANK) at increasing concentrations of RANKL, **as indicated.** **(D)** Receptor half-life study in HEK-RANK cells treated with cycloheximide (CHX) and Pep8 (200  $\mu$ M) or RANKL, as indicated. Immunoblots were probed with an antibody against human RANK/TNFRSF11A.  $\beta$ -Actin served as control. **For all experiments, representative blots are shown. Bar graphs show relative densitometric values and represent the means  $\pm$  SD of three independent experiments. **\*\*\* $p < 0.001$ , \*\* $p < 0.01$  and \* $p < 0.05$ .****

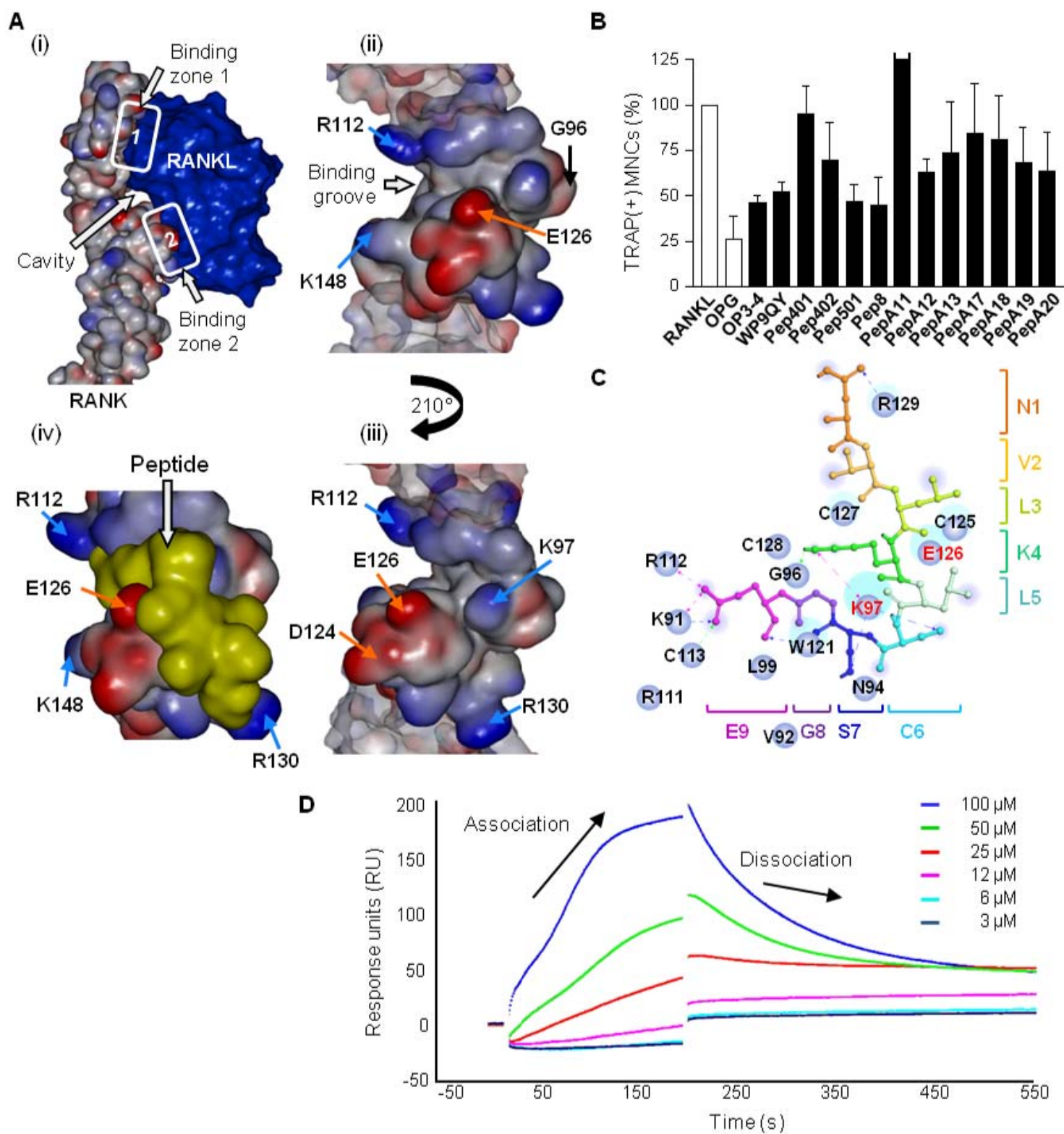
**Fig. 5.** Inhibitory effect of Pep8 on ovariectomy-induced bone loss. (Left columns) Representative three-dimensional transversal  $\mu$ CT images of the proximal region of tibiae and 4<sup>th</sup> lumbar vertebrae from mice treated with 10 mg/kg/d Pep8, vehicle (OVX) or healthy controls (NOV) (n = 8/group). (Middle column) Masson's trichrome staining of longitudinal sections from proximal tibiae. Green stain indicates bone tissue and reddish-brown stain soft tissues. (Right column) Positive TRAP staining of osteoclasts (stained in red) on areas of resorption along the growth plate region in tibia sections. Scale bars, 0.8 mm.

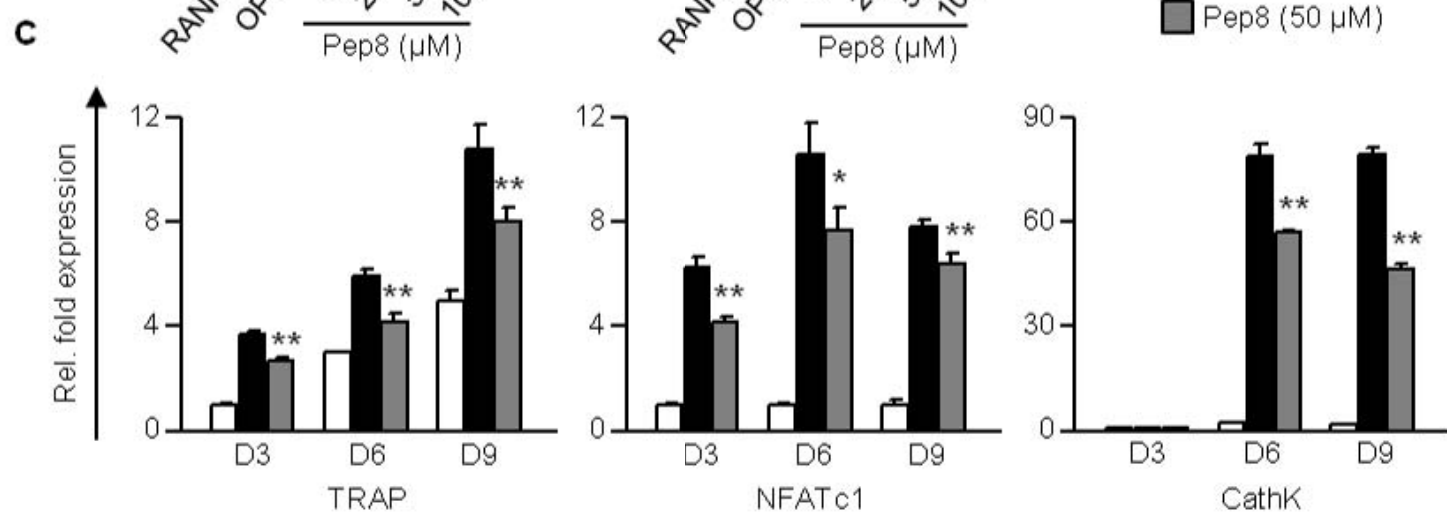
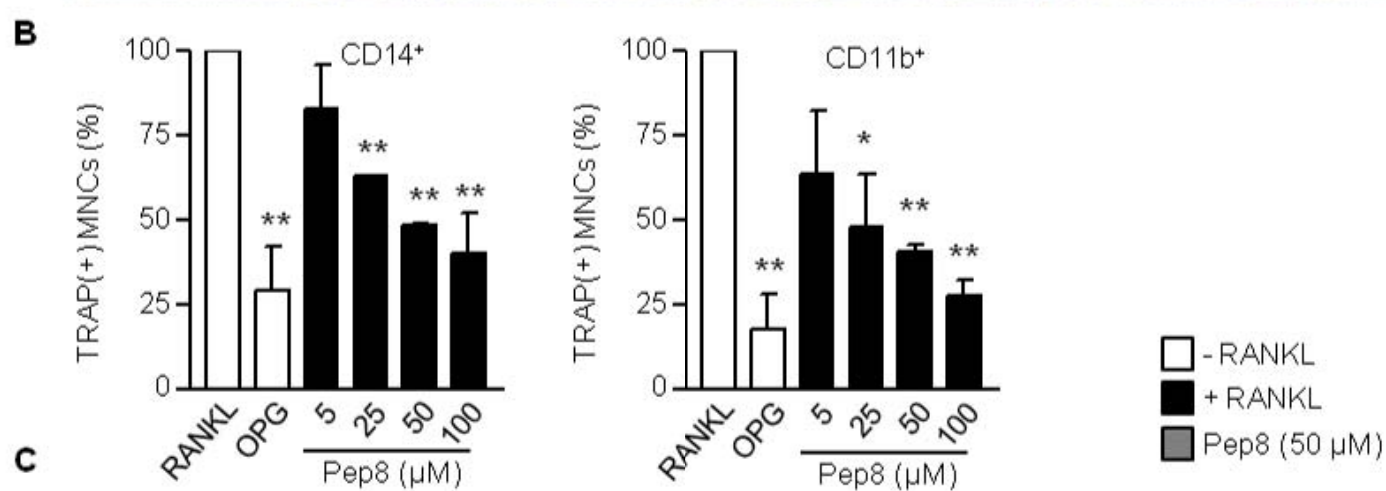
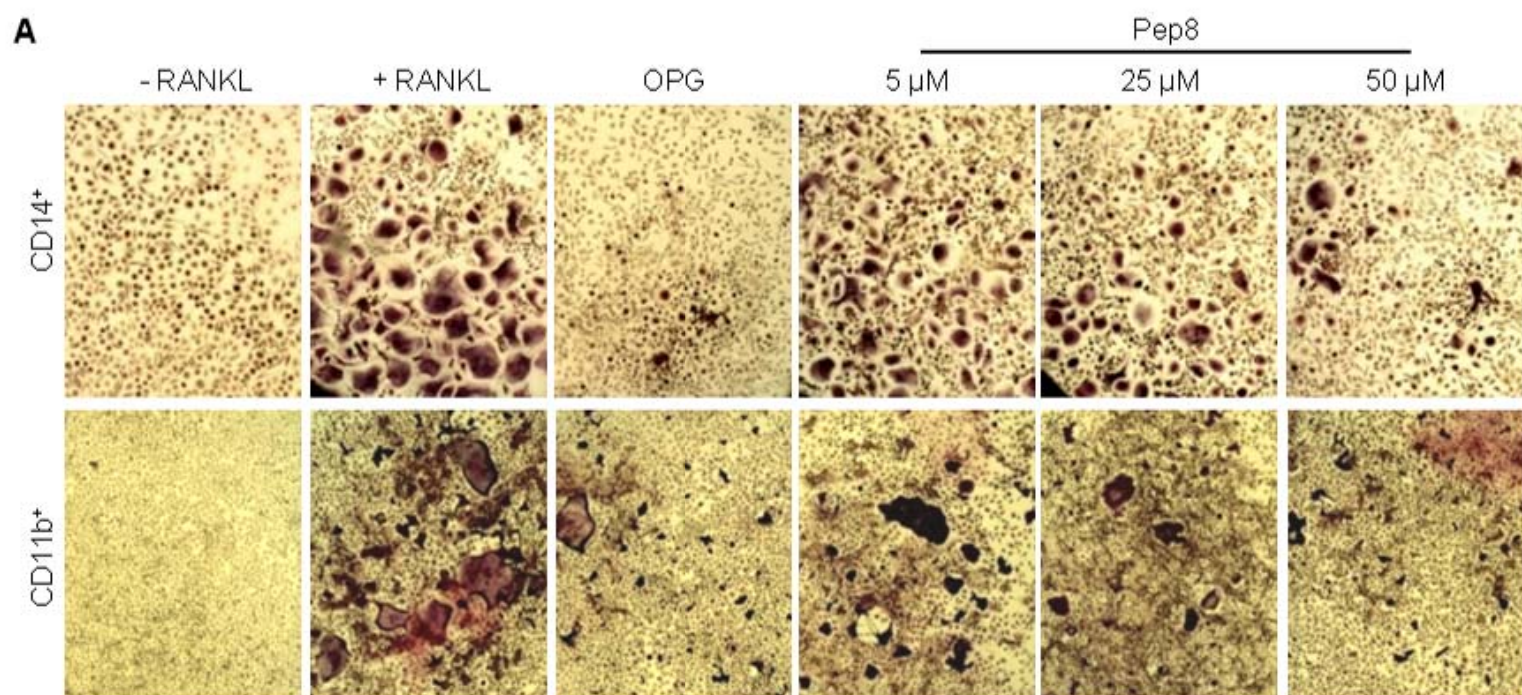
**Fig. 6.** Peptide-target interaction of Pep8 and screening of Pep8 derivatives. **(A)** Expansion of the region containing resonances of the amide protons of Pep8 in association with RANK: reference 1D <sup>1</sup>H (black) and 1D <sup>1</sup>H STD-NMR spectrum (red), showing enhancements of resonances of protons making close contacts with the interaction site on the receptor. STD values are obtained after peak picking intensities compared with the 1D, with the exact values of chemical shifts of the NH (AAs in bold have intense relative STD). **(B)** Relative STD intensities for the individual NH protons of Pep8 normalized to K4 were used to compare the STD effect. **(C)** In vitro activity of Pep8 derivatives. Peptide activity was arbitrarily classified in three categories (dotted lines), with an activity zone signifying similar activity to Pep8. Peptide length varies between 5 and 14 amino acids. Black bars, good binding predicted in silico; light grey bars, low or unclear binding prediction.

**Table 1.** Histomorphometric analysis of the protective effect of Pep8 on ovariectomy-induced bone loss

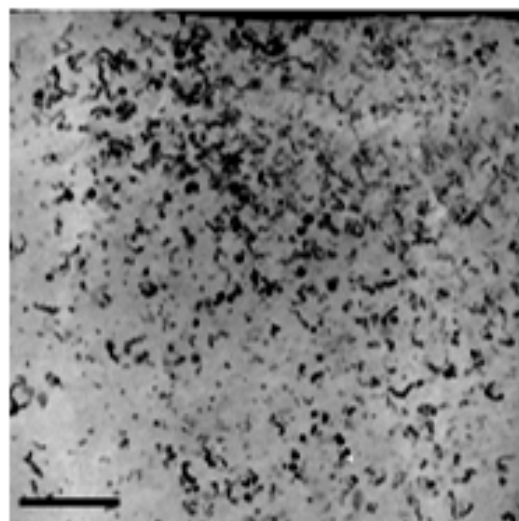
Parameter	NOV	OVX	Pep8
<i>Proximal tibia, trabecular</i>			
BV/TV (%)	15.05 ± 1.09	5.97 ± 0.74 <sup>c</sup>	11.51 ± 1.15 <sup>a,d</sup>
TbTh (µm)	99.71 ± 1.39	88.11 ± 3.23 <sup>d</sup>	100.34 ± 3.06 <sup>a</sup>
TbN (1/mm)	1.50 ± 0.09	0.66 ± 0.07 <sup>c</sup>	1.13 ± 0.09 <sup>a,c</sup>
TbS (µm)	406.6 ± 24.2	628.5 ± 17.9 <sup>d</sup>	506.4 ± 24.4 <sup>a,c</sup>
<i>Vertebral body, trabecular</i>			
BV/TV (%)	47.06 ± 1.02	33.21 ± 1.21 <sup>c</sup>	37.47 ± 1.41 <sup>b,c</sup>
TbTh (µm)	125.3 ± 1.44	112.9 ± 1.45 <sup>c</sup>	116.1 ± 2.55 <sup>c</sup>
TbN (1/mm)	3.75 ± 0.06	2.94 ± 0.07 <sup>c</sup>	3.22 ± 0.07 <sup>b,c</sup>
TbS (µm)	202.2 ± 5.77	262.0 ± 6.61 <sup>c</sup>	238.7 ± 7.53 <sup>b,c</sup>

Data are expressed as mean ± SEM. BV/TV, bone volume/tissue volume ratio; TbTh, trabecular thickness; TbN, trabecular number; TbS, trabecular spacing; <sup>a</sup>*p* < 0.01 and <sup>b</sup>*p* < 0.05 vs. OVX group; <sup>c</sup>*p* < 0.01 and <sup>d</sup>*p* < 0.05 vs. NOV group using ANOVA and Dunnett's posttest.

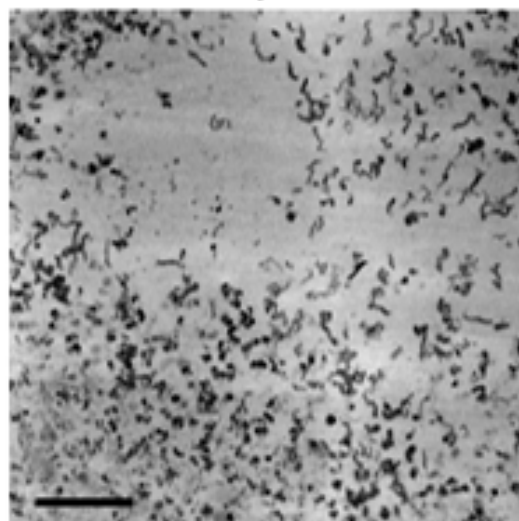




RANKL

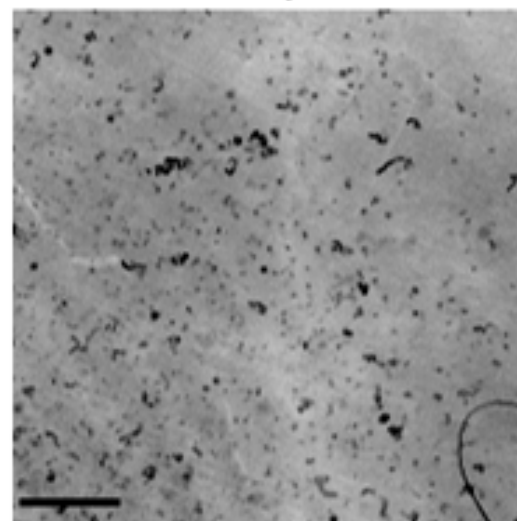


50  $\mu$ M



Pep8

100  $\mu$ M



300  $\mu$ M

